

# “COHERENCE RADAR” AND “SPECTRAL RADAR”—NEW TOOLS FOR DERMATOLOGICAL DIAGNOSIS

Gerd Häusler and Michael Walter Lindner

University of Erlangen-Nürnberg, Physics Institute, Chair for Optics, Staudtstr. 7/B2, 91058 Erlangen, Germany

(Paper JBO/IB-010 received August 13, 1997; revised manuscript received Nov. 16, 1997; accepted for publication Nov. 27, 1997.)

## ABSTRACT

“Coherence radar,” an optical 3-D sensor based on short coherence interferometry, is used to measure skin surface topology. This method is called optical coherence profilometry (OCP) and it may be a useful tool for medical diagnosis in dermatology because different medical conditions show distinct alterations of the skin surface. The measuring uncertainty is less than  $2\ \mu\text{m}$ . The measuring time is about 4 s. *in vivo* 3-D mapping of naked skin was performed without preparation. For clinical application, a fiber optical implementation was introduced. Spectral radar is an optical sensor for the acquisition of skin morphology based on OCT techniques. The scattering amplitude  $a(z)$  along one vertical axis from the surface into the bulk can be measured within one exposure. No reference arm scanning is necessary. The theory of the sensor, including the dynamic range, is discussed and *in vivo* measurements of human skin by a fiber optical implementation of the sensor are demonstrated. © 1998 Society of Photo-Optical Instrumentation Engineers. [S1083-3668(98)01801-2]

**Keywords** optical coherence profilometry; optical coherence tomography; speckle interferometry; coherence radar; spectral radar; Fourier spectroscopy; human skin; melanoma maligna; *in vivo* measurements; volume scatterers.

## 1 INTRODUCTION

An important medical aim in experimental dermatology is to quantitatively measure pathological alterations of the skin in a very early state, as well as to quantify the influence of pharmacological and cosmetic preparations. On one hand these alterations occur at the surface of the skin: in its topology and texture. On the other hand, they cause changes in the volume of the skin, such scattering characteristics in the different layers of the skin. Skin cancer, for example, causes a flattening of the skin surface; the typical wrinkles vanish. In addition, an increased backscattering occurs in the volume of the skin through the accumulation of melanin in the cells.

One feature of cosmetic preparations is that they increase the moisture content in the top layers of the skin. This leads to an extension of the epidermis, and therefore to a reduction of wrinkles. Such effects have to be investigated with an accuracy of a few microns. We demonstrate methods to measure both surface topology as well as morphological data. These methods consist of optical coherence profilometry (OCP) for the acquisition of the sur-

face skin topology and optical coherence tomography (OCT) for the acquisition of morphological 3-D data from the volume of the skin.

## 2 OPTICAL COHERENCE PROFILOMETRY BY COHERENCE RADAR

### 2.1 INTRODUCTION

Pathological alterations of human skin can occur in both the volume of the skin and in its topology. Superficial alterations in the texture of the skin, as for example, atrophy, can be caused by melanoma maligna. Methods for characterizing the surface relief of the skin by texture analysis are well established. However, these methods are either based on fringe projection, with a measuring uncertainty of about  $20\ \mu\text{m}$ , or they are based on measurements of silicone replicas of the skin. The replica is observed via a microscope, photographed with a CCD camera, and subsequently subjected to image analysis by a digital computer.<sup>1</sup> Then the information on texture is encoded in gray-level images of the surface. This procedure takes about 20 min and delivers 2-D data on the texture. For quantitative analysis, actual 3-D-data of the topology of the skin are required.

Address all correspondence to Michael Walter Lindner, Physikalisches Institut der Universität Erlangen-Nürnberg, Lehrstuhl für Optik, Staudtstr. 7/B2, 91058 Erlangen. Tel.: 49 9131 858384; Fax.: 49 9131 13508; E-mail: mwl@physik.uni-erlangen.de

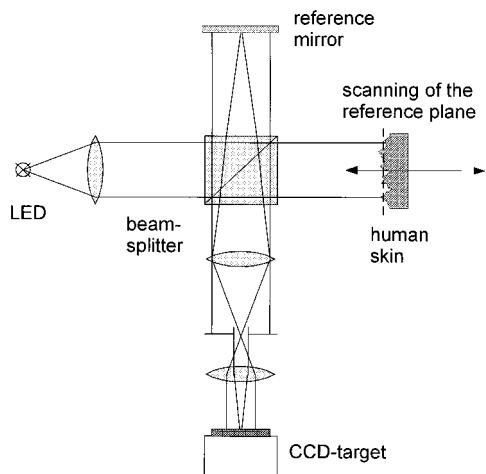


**Fig. 1** Experimental setup of the coherence radar.

Another commonly used method for measuring replicas consists of tactile sensors. These sensors deliver actual 3-D data but the measuring time needed is significant (30 min). The drawback of methods that are based on the measurement of a replica is that the making of the replica itself causes artifacts in the topology.

We introduced a sensor based on short coherence interferometry, the "coherence radar"<sup>2</sup> for topography. These sensors are well established for measuring industrial objects.<sup>3,4</sup> We adapted the coherence radar for biological objects and were able to measure the 3-D topology of human skin with an uncertainty of less than  $2 \mu\text{m}$ .<sup>5,6</sup> The measuring time is only a few seconds.

## 2.2 MEASURING PRINCIPLE

The experimental setup of the coherence radar is a Michelson interferometer (Figure 1). The light source is a light-emitting diode (LED). The reference mirror and the skin are illuminated by a plane wave. The light that is scattered back from the surface of the skin is imaged onto the CCD camera. Imaging with a finite aperture causes speckle in the image plane. Each speckle has a constant phase. Therefore the speckles are the actual signal carrier in interferometry on rough surfaces.<sup>2</sup>

White light interference displays maximum contrast in a plane, where an object's optical path length is equal to the reference path length. To get a 3-D shape, the reference plane has to be scanned through the object. During the scan in each pixel of the CCD camera, an intensity variation occurs, called a *correlogram* [Figure 2(a)]. Its period is half of the average wavelength of the light source.

For each pixel, the contrast of the correlogram is measured during the scan. The maximum contrast defines the locus of equal optical path lengths. Outside the center, the interference contrast decays rapidly, depending on the coherence length of the light

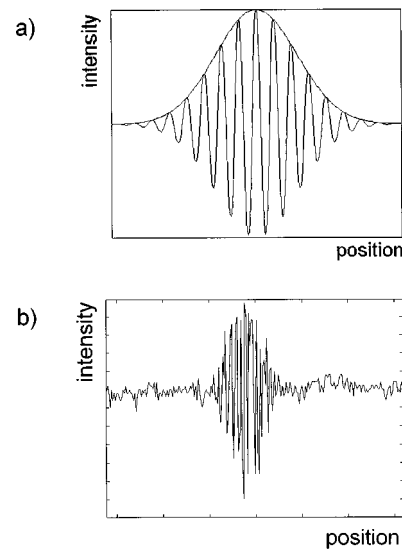


**Fig. 2** (a) Theoretical correlogram of interference intensity versus  $z$  position. (b) Correlogram of an *in vivo* measurement of human skin.<sup>6</sup>

source. Special hardware is used to detect this maximum and to save the actual position of the translation stage. This is done for each of the 256,000 pixels of the frame in parallel. The speed of depth measurement is  $v_s = \lambda/6T$ , which is  $4 \mu\text{m/s}$  using a standard video camera with a 25-Hz frame rate. By modifying the sensor, the speed can be increased up to  $70 \mu\text{m/s}$ .<sup>6</sup>

The uncertainty  $\delta z$  (standard deviation) in measurements with the continuous coherence radar is caused by the statistical phase in the speckle. Therefore  $\delta z$  is mainly limited by the roughness of the object and not by parameters of the sensor (e.g., observation aperture). Industrial surfaces can be measured with  $\delta z < 1 \mu\text{m}$ .<sup>2</sup>

The algorithm is based on measuring the contrast of the correlogram, not its phase. Thus movements of the object that could distort the phase will not influence the contrast. This is why *in vivo* measurements of a slightly moving object such as human skin are possible.

## 2.3 MEASUREMENTS ON HUMAN SKIN WITHOUT PREPARATION

In order to measure the topology of human skin *in vivo* with the coherence radar, up until now we had to prepare the skin with graphite powder. We used this preparation for two reasons: First we had to increase the reflectivity to get a sufficiently high signal contrast, even from the thin wrinkles. Second, skin is a volume scatterer, which means that the light penetrates the volume and is scattered back from the deep bulk. Therefore the highest contrast would be measured in the upper layers of the skin and not exactly at the surface. With the help of the graphite preparation, we could measure only

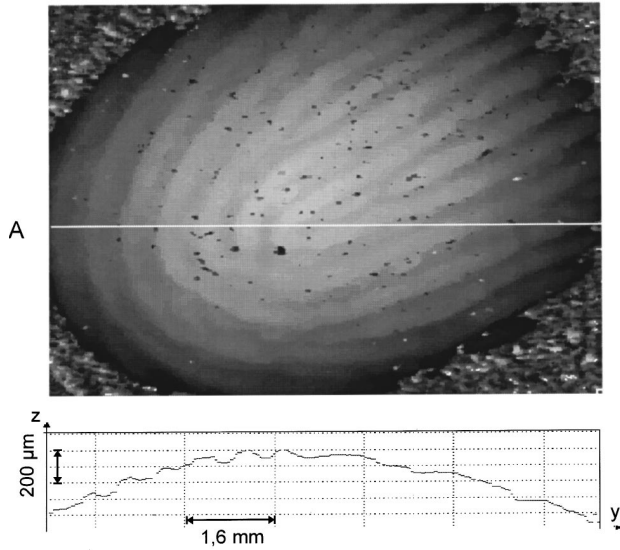


**Fig. 3** *In vivo* topology of a fingertip measured with the coherence radar. The surface reflectivity was increased by graphite. The top image displays a gray-level encoded height map and the bottom image shows the profile along the line A.<sup>6</sup>

the signal from the surface of the skin. Owing to the increased reflectivity, the power of the LED was sufficient to illuminate a field of  $7 \times 10 \text{ mm}^2$ . However, since the coherence radar has to scan the depth of the whole object with a limited velocity, the measuring time of these earlier measurements was long (about 150 s). Figure 3 shows an *in vivo* measurement of a prepared fingertip with the coherence radar.

For cosmetic and medical applications, any kind of preparation should be avoided because it causes artifacts, which means that the measured results do not correspond to the actual 3-D topology. We avoid having to use the preparation by focusing the light source onto the measured part of the skin. Then we get sufficiently high signal contrast, even at the bottom of the thin wrinkles. However, the measured field decreases to about  $1.4 \times 1.4 \text{ mm}^2$  due to the focusing.

In order to examine the influence of the bulk signal, we compared measurements on prepared skin and naked skin. Figure 4(a) shows the intensity plot of a measured area on the underarm. The prepared area can be seen in the lower part as the brighter area. In the upper part of Figure 4(a), there is naked skin. A magnification of the boundary area can be seen in Figure 4(c). The result of the OCP measurement of this part of the body is shown as a gray-level encoded height map in Figure 4(b). Figure 4(d) displays a magnification of the boundary area. (The profiles are displayed below each height map along the lines A and B, respectively.) In Figure 4(d) the profile along the line B shows that there is

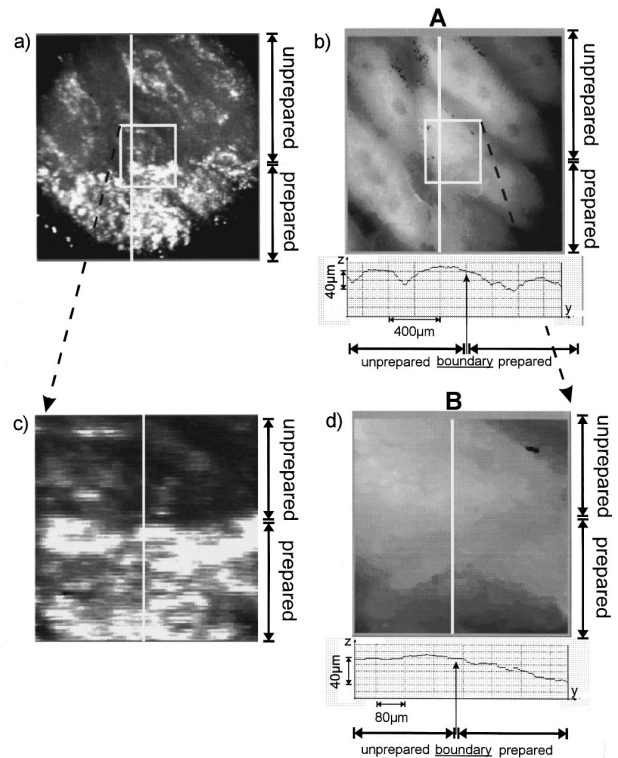


**Fig. 4** Comparison between measurements of naked skin and skin prepared with a thin graphite layer.<sup>6</sup> (a) Intensity plot of the measured area. The prepared area can be seen in the lower part, where the signal is brighter. (b) Gray-level encoded height map. (c) Magnification of the boundary area in (a). (d) Magnification of the boundary area of the height map (the profiles are displayed below each height map along the lines A and B, respectively). There is no change in the height at the boundary between the prepared and naked skin.

no change in the height at the boundary between prepared and naked skin. That means that the coherence radar is not disturbed by the bulk signal. Therefore we can perform *in vivo* OCP measurements without preparation of the skin.

In order to confirm this result, we also measured the interferometric signal seen by one camera pixel during an *in vivo* measurement of human skin as a function of the  $z$  value of the translation stage [Figure 2(b)]. Compared with the theoretical interferogram [Figure 2(a)], the measured interferogram shows some camera noise and some phase shifts in the signal. These phase shifts were caused by trembling of the test person during the measurement. Nevertheless, the interferogram shows a contrast maximum that can be localized. Since the coherence radar is an interferometer that does not utilize the phase of the signal but only the contrast, unavoidable trembling of the patient by a couple of wavelengths will not disturb the measurement. This is why we can perform interferometrical *in vivo* measurements with the coherence radar.

Thus we can perform *in vivo* measurements of human skin without preparation. This is interesting because working with replicas leads to artifacts, as

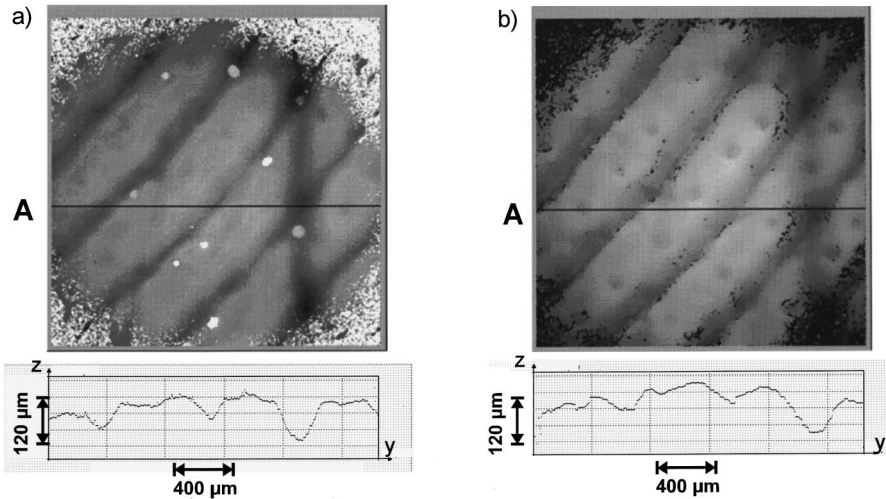


**Fig. 5** Comparison between (a) silicone replica and (b) *in vivo* measurement of the same area (top: gray-level encoded height map; bottom: profiles of the height map along the line A).<sup>6</sup>

shown in Figure 5. We compared the measurement of a silicone replica [Figure 5(a)] and an *in vivo* measurement of the same area [Figure 5(b)] with the coherence radar. The white circles in Figure 5(a) are artifacts caused by the fact that the test person transpired while the silicone was hardening. The *in vivo* measurement does not show any artifacts. Making the replica takes 10 min and measuring it with a tactile sensor takes about 30 min. The *in vivo* measurement takes only 5 s.

We performed *in vivo* measurements of different areas with the coherence radar (Figure 6). The field of view was  $1.4 \times 1.4 \text{ mm}^2$ . The measuring times depend on the depth in scanning. With a scanning speed of  $14 \mu\text{m/s}$ , the measuring time takes about 5 to 10 s. All measurements were performed *in vivo* without any preparation of the skin.

The measurement of the forearm [Figure 6(a)] displays deep wrinkles about  $60 \mu\text{m}$  in depth and shallow wrinkles about  $30 \mu\text{m}$  in depth. The coherence radar allows us to examine the depth of these wrinkles with an uncertainty of less than  $2 \mu$  of standard deviation. The cosmetic industry is interested in this feature because shallow wrinkles vanish more and more with the age of the skin. So we are able to investigate the effects of cosmetic products on this process. Figure 6(b) shows the wrinkles and the perspiratory glands of the hand, which have a depth of about  $30 \mu\text{m}$ .

#### 2.4 CLINICAL RELEVANCE

The topology of human skin is interesting not only for cosmetic reasons but also has clinical relevance.

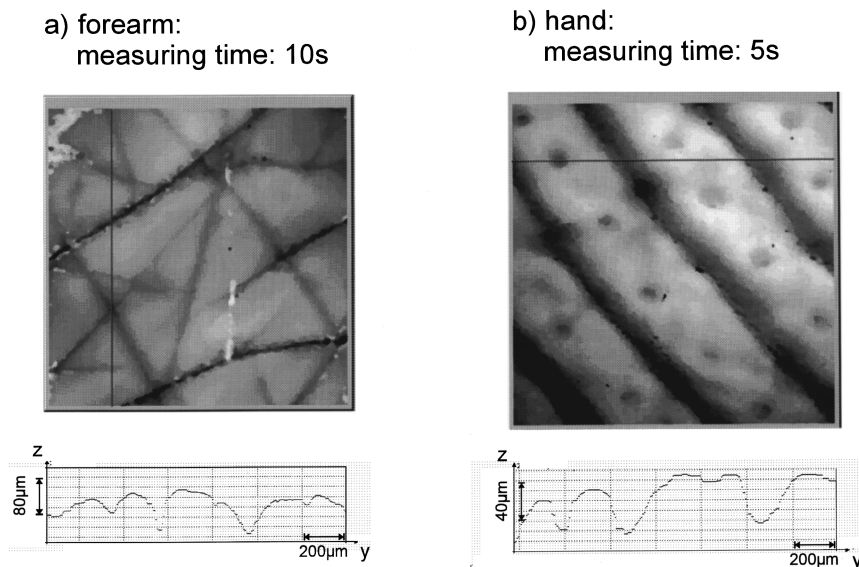


**Fig. 6** *In vivo* OCP measurements of naked skin by coherence radar (a) forearm, measuring time, 10 s and (b) hand, measuring time, 5 s.

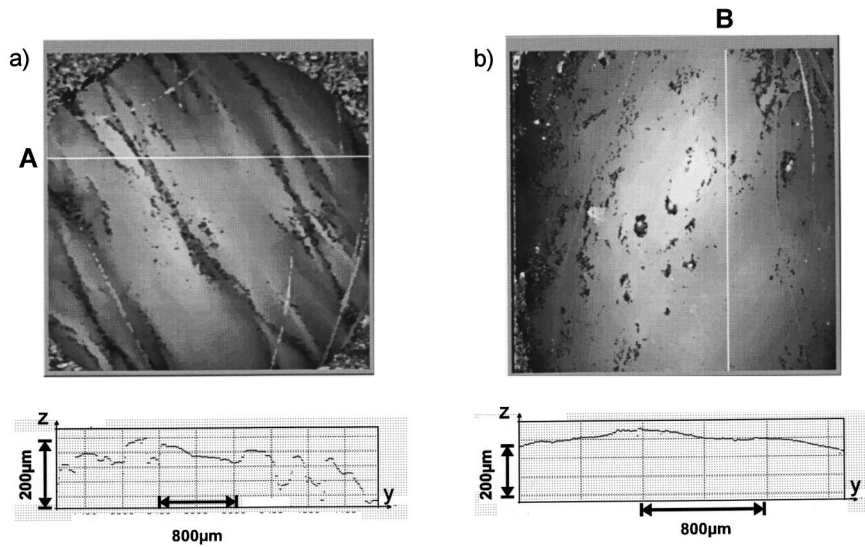


**Fig. 7** Comparison between (a) normal skin and (b) Morbus Bowen.<sup>6</sup>

Alterations of the skin such as the process of wound healing, the secondary effect of cortisone application, and alterations caused by skin cancer are encoded in the topology of the skin surface as well. As an example, we show a comparison between healthy skin and a Morbus Bowen. The normal skin [Figure 7(a)] shows a characteristic texture with fine wrinkles. These wrinkles do not occur in the topology of the Morbus Bowen [Figure 7(b)].

### 2.5 FIBER OPTICAL IMPLEMENTATION

Since the conventional setup of the coherence radar is bulky, the area of the human body to be measured has to be brought to the sensor. To bring the sensor to the body, we implement the coherence radar by fiber optics.<sup>6</sup> By doing this, the bulky translation stage, which makes the scan in the z-direction, can be placed far away (under the table) from the sensor head, which can then be miniaturized. We implement the concept by illuminating the object via an object fiber and by sending the reference wave through a reference fiber. The path length is modulated by a linear translation stage that is separated from the small mobile sensor head.

### 2.6 SUMMARY

Different modifications of white light interferometry have been used for 3-D mapping of the human skin. We performed *in vivo* OCP measurements of skin topology without preparation by using coherence radar. We achieved an uncertainty of less than  $2 \mu$  with typical measuring times of 5 s. In addition, we demonstrated the clinical relevance of the measurements because we can clearly distinguish the topology of the surface of a Morbus Bowen and normal skin. A miniaturized coherence radar system will be implemented by fiber optics.

## 3 OPTICAL COHERENCE TOMOGRAPHY BY SPECTRAL RADAR

### 3.1 INTRODUCTION

In order to investigate morphological 3-D data in biological objects, methods based on optical coherence tomography have become more and more important during the past few years. The OCT methods can be divided into two classes: sensors based on time domain measuring principles and those based on Fourier domain principles.

Time domain principles of OCT use a broad bandwidth light source in an interferometric setup. Interference contrast is detected only if the object path length equals the reference path length. The path length of the photons to be detected (backscattered from the tissue) can be adjusted by the reference path length. Therefore the reference path has to be scanned through the depth range. Time domain methods have been investigated in a multitude of modifications.<sup>5,7-15</sup>

Fourier domain principles avoid scanning the reference through the depth range. These OCT sensors obtain depth information by evaluating the spectrum of the interferogram. The Fourier transformation of the spectrum delivers the depth information. For this type of sensor, there are several approaches. On the other hand a broad bandwidth light source is used for the illumination of the interferometer. The interferometer output is spectrally resolved and the whole spectrum is detected by an array of photodiodes. This specific implementation can be adapted for measurements on the (transparent) eye<sup>9,10,15</sup> as well as for measurements of strongly scattering skin.<sup>16-18</sup> In a further modification, the spectrum can be produced by a tunable laser and then be detected by a single photodiode.<sup>19,20</sup> In both classes of OCT sensors,

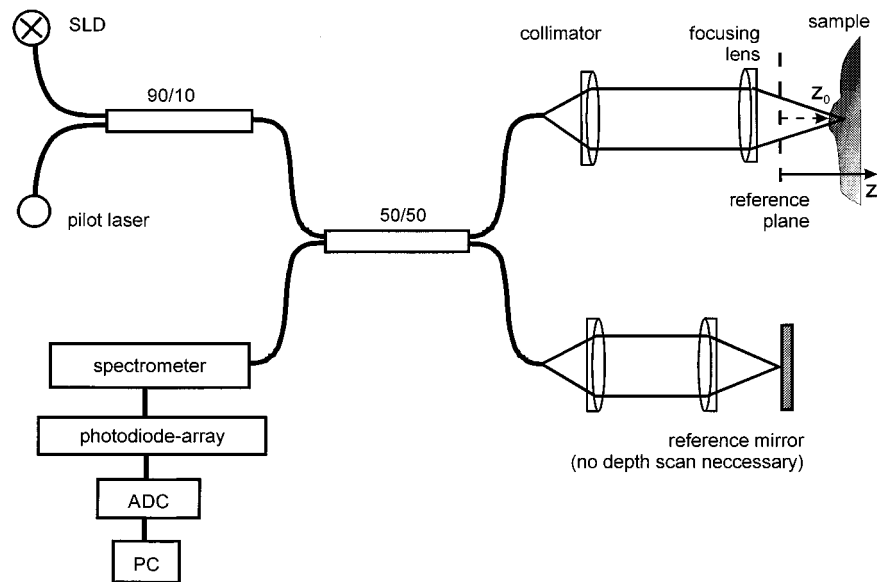


**Fig. 8** Fiber optical implementation of the spectral radar.

time and Fourier domain, the speckle contrast is the actual source of information.<sup>21,22</sup>

### 3.2 EXPERIMENTAL SETUP

Spectral radar measures the scattering amplitude  $a(z)$  along one vertical axis from the surface into the bulk within one exposure. No scanning of the reference arm is necessary. For two-dimensional imaging, a transverse scanning is necessary. In order to perform *in vivo* measurements on different locations of the human body, the spectral radar is implemented by single-mode fiber techniques.

The sensor is a modified Michelson interferometer (Figure 8). The light source is a SLD [central wavelength:  $\lambda = 840$  nm, full width at half-maximum (FWHM) = 20 nm, coherence length:  $l_C = 35$   $\mu\text{m}$ ; output power  $P = 1.7$  mW]. In order to localize the point of the measurement on the skin, we use an additional pilot laser in the visible range. The light is directed into the object beam and the reference beam by a 50:50 fiber coupler.

We focus the beam in the reference arm onto a reference mirror. The same combination of lenses is used in the object arm to focus the light onto the skin. We use this combination to have 2 deg of freedom in the setup. First we need to adjust the optical path length in both arms. The reference plane is positioned at a distance  $z_0$  of about 200  $\mu\text{m}$  in front of the object surface in order to get rid of the source spectrum (correlogram) and the autocorrelation terms (described later). Second, we can vary the position of the focus of the illumination beam within the skin. The light is focused into the skin at a depth of about 200  $\mu\text{m}$ . The diameter of the spot at the surface is about 50  $\mu\text{m}$  and the power in the focus is about 360  $\mu\text{W}$ . The focus is placed into the

skin in order to enhance the interference contrast in deeper regions of the object.<sup>8</sup> The waves scattered back from different depths of the object are coaxially observed.

Imaging with a finite aperture causes subjective speckle at the entrance of the fiber. The speckle contrast is the actual carrier of the information. With an aperture of N.A. = 0.1 of the fiber core, there is only one speckle on the core. The confocal imaging of the backscattered photons onto the fiber core also has the advantage of a spatial separation of the photons. For photons that have been scattered often, there is hardly any correlation between the run time and the depth information. Now these photons will no longer hit the fiber.

The backscattered waves are superimposed on the reference wave. At the interferometer exit we locally separate the different wavelengths by a grating spectrometer with a resolution of 0.05 nm. The spectrum is imaged onto an array of 1024 photodiodes. The size of each photodiode is 2.5 mm  $\times$  20  $\mu\text{m}$ . Each photodiode can collect  $9 \times 10^7$  photons to give a low photon shot noise and a large dynamic range. The signal is transferred to the host computer by a 14-bit A/D converter. There the Fourier transformation is performed.

### 3.3 MEASURING PRINCIPLE

The measuring principle is based on spectral interferometry. The signal from the object consists of many elementary waves emanating from different depths  $z$ . We neglect the dispersion in the object. The scattering amplitude of the elementary waves versus depth is  $a(z)$ . The object signal is superimposed on the plane reference wave  $a_R$ . At the exit

of the interferometer, we locally separate the different wave numbers  $k(=2\pi/\lambda)$  by a spectrometer. The interference signal  $I(k)$  is

$$I(k) = S(k) \left| a_R \exp(i2kr) + \int_0^\infty a(z) \times \exp\{i2k[r+n(z)\cdot z]\} dz \right|^2, \quad (1)$$

where

- $2r$  = path length in the reference arm (because we care only about path differences, we define  $r=0$  arbitrarily),
- $2(r+z)$  = path length in the object arm,
- $2z$  = path length in the object arm, measured from the reference plane (Figure 8),
- $z_0$  = offset distance between the reference plane and object surface (Figure 8),
- $n$  = refractive index ( $n=1$  for  $z < z_0$  and  $n \approx 1.5$  for longitudinal positions in the object  $z > z_0$ ),
- $a_R$  = amplitude of the reference (for further investigations we set  $a_R=1$ ),
- $a(z)$  = backscattering amplitude of the object signal; with regard to the offset  $z_0$ ,  $a(z)$  is zero for  $z < z_0$  (Figure 9), and
- $S(k)$  = spectral intensity distribution of the light source.

With these assumptions, the interference signal  $I(k)$  can be written as

$$I(k) = S(k) \left| 1 + \int_0^\infty a(z) \exp(i2knz) dz \right|^2 \quad (2)$$

$$= S(k) \left[ 1 + 2 \int_0^\infty a(z) \cos(2knz) dz + \int_0^\infty \int_0^\infty a(z) a(z') \exp[-i2kn(z-z')] dz dz' \right]. \quad (3)$$

It can be seen that  $I(k)$  is the sum of three terms. Besides a constant offset, the second term encodes the depth information of the object. It is a sum of cosine functions, where the amplitude of each cosine is proportional to the scattering amplitude  $a(z)$ . The depth  $z$  of the scattering event is encoded in the frequency  $2nz$  of the cosine function. This term describes the well-known Müller fringes in spectral interferometry.<sup>23</sup> It will be seen that  $a(z)$  can be acquired by a Fourier transformation of the interferogram.<sup>24</sup> The third autocorrelation term describes the mutual interference of all elementary waves.

We can get  $a(z)$  by Fourier transformation of  $I(k)$  under the assumption that  $a(z)$  is symmetric with respect to  $z$ . Fortunately  $a(z)=0 \forall z < z_0$ . So we can replace  $a(z)$  by the symmetric expansion  $\hat{a}(z) = a(z) + a(-z)$ . After the Fourier transformation we have to restrict ourselves to  $z > z_0$ , which gives us the depth information of the object.

$$I(k) = S(k) \left[ 1 + \int_{-\infty}^\infty \hat{a}(z) \cos(2knz) dz + \frac{1}{4} \int_{-\infty}^\infty \int_{-\infty}^\infty \hat{a}(z) \hat{a}(z') \exp[-i2kn(z-z')] dz dz' \right] \quad (4)$$

$$I(k) = S(k) \left[ 1 + \int_{-\infty}^{+\infty} \hat{a}(z) \exp(-i2knz) dz + \frac{1}{4} \int_{-\infty}^{+\infty} AC[\hat{a}(z)] \exp(-i2knz) dz \right]. \quad (5)$$

In this notation  $AC[\hat{a}(z)]$  is the autocorrelation.

$$I(k) = S(k) \left( 1 + \frac{1}{2} FOU_z \{ \hat{a}(z) \} + \frac{1}{8} FOU_z \{ AC[\hat{a}(z)] \} \right). \quad (6)$$

Performing the inverse Fourier transformation we get

$$FOU^{-1}\{I(k)\} = FOU^{-1}\{S(k)\} \otimes ([\delta(z)] + \frac{1}{2}\hat{a}(z) + \frac{1}{8}AC[\hat{a}(z)]) = A \otimes (B + C + D) \quad (7)$$

( $\otimes$  indicates convolution).

From this result, the symmetrized scattering amplitude  $\hat{a}(z)$  and therefore  $a(z)$  can be deduced; in other words, we can see the strength of the scattering versus the depth.

However, besides the signal term  $C$  there are three further terms in Eq. (7):  $A$ ,  $B$ , and  $D$ . These terms are well known from holography. As in holography, we can get rid of them by an offset  $z_0$  of the reference plane to the object surface. In the first term,  $A \otimes B$ , we get the Fourier transformation of the source spectrum (correlogram= $A$ ) located around  $z=0$ . To separate the correlogram  $A$  from the signal  $C$ , we place the reference  $200 \mu\text{m}$  in front of the surface of the object. This is sufficient for the separation, since the correlogram is much shorter (coherence length  $\sim 35 \mu\text{m}$ ).

There is one more disturbing term:  $A \otimes D$ .  $D$  are the autocorrelation terms, which describe the mutual interference of all scattered elementary waves. In strongly scattering skin, the influence of  $D$  is negligible, because the autocorrelation term is much weaker than the signal term, which is

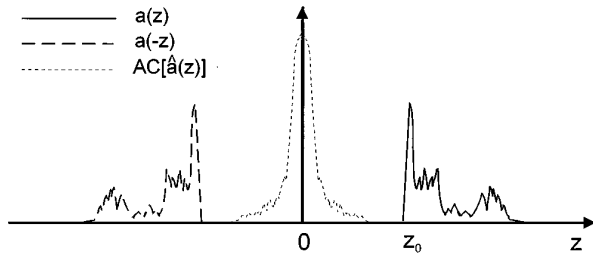


**Fig. 9** Sketch of the scattering amplitude  $a(z)$  and the AC terms.  $a(z)$  is zero up to the object surface that is located at  $z_0$ . Owing to the reference offset  $z_0$ , the object reconstruction is separated from the AC terms, which are located around  $z=0$ .

weighted by the strong reference amplitude. Moreover, these terms are located around  $z=0$ . Therefore, the center of the AC term is separated from the object signal  $a(z)$ , even for a small offset  $z_0$  (Figure 9). As mentioned, the outer lobes of the AC terms are too weak to disturb the results. If the object shows high backscattering from large depths, there is still the possibility of performing a second measurement at each position with no reference signal, and subtracting that signal from  $I(k)$ .

Finally, we have a convolution of the signal  $C$  with the correlogram of the light source. In order to achieve high-resolution measurements, the spectral characteristics of the light source have to be taken into account. Only if the light source has a broad and smooth spectrum without noise or ripple will the convolution peaks be sufficiently narrow.

### 3.4 MEASURING RANGE AND UNCERTAINTY

The measuring range  $\Delta z$  of the spectral radar is limited by the resolution of the spectrometer.<sup>17</sup> A large difference in the optical paths of object and reference will cause a high frequency in the spectrum. According to the sampling theorem, the sample frequency of the photodiode array has to be twice as large as the highest occurring frequency in the spectrum. For  $z = z_{MAX}$ , the period of the cosine fringes is:  $\delta k = \pi / n z_{MAX}$ . Therefore the spectrometer has to resolve at least  $\delta k / 2$ . With  $|\delta k| = 2\pi \delta \lambda / \lambda^2$ , we get

$$\Delta z = \frac{1}{4n} \frac{\lambda^2}{\delta \lambda}. \quad (8)$$

With the parameters in our setup, the measuring range is  $\Delta z = 2.4 \text{ mm}$  ( $n = 1.5$ ).

However, if we measure a mirror at variable distance  $z$ , we observe a Gaussian decay of the signal peak with increasing distance. This decay is caused by the limited spectral resolution ( $1/\delta \lambda$ ) of the spectrometer, although the reflected amplitude stays the same. In order to obtain the real scattering amplitude  $a(z)$ , we first have to compensate for

this decay by normalization. Each measurement is normalized by dividing the measured signal by the measured Gaussian decay.

The achievable spatial resolution depends on the coherence length of the light source and the scattering characteristics of the object. According to our experiments on the behavior of the spatial impulse response during signal propagation in volume scatterers with OCT methods,<sup>21</sup> the minimum resolvable distance decreases with decreasing coherence length. However, it is finally limited by the scattering characteristics of the object. In order to determine the spatial resolution of the spectral radar, we measured a well-defined multilayer object with scattering coefficients adapted to human skin.<sup>5</sup> It turns out that the achievable spatial resolution within a range of  $1000 \mu\text{m}$  is about  $10 \mu\text{m}$ .

### 3.5 DYNAMIC RANGE

An important feature of spectral radar is its dynamic range  $D$ . In order to perform measurements in strongly scattering objects like human skin, a high dynamic range is needed. In OCT methods, the speckle contrast is the actual source of information.<sup>21</sup> Therefore the principal problem is to detect the small speckle contrast, which is riding on a high incoherent background. The question is: How small can an interference signal be to be still detected on the large background? From these considerations it follows that we need a large, full well capacity of our photodiode array to get a high ratio of signal-to-photon shot noise.

First we have to consider the noise. In our setup (with  $360 \mu\text{W}$  on the object), we reach the saturation of the photodiode array with exposure times in the range of 10 to 400 ms (depending on the object). We measure near the saturation of the camera; hence the shot noise is the dominating source of noise. Dark current noise and readout noise are negligible. We use a photodiode array with large diodes ( $2.5 \text{ mm} \times 20 \mu\text{m}$ ) to accumulate as many photons as possible ( $9 \times 10^7$  photons in each diode). Then we achieve the best ratio between signal and noise. The price we have to pay is an exposure time in the range of 100 ms, because we have to saturate 1024 large diodes.

In a first approximation we can formulate the following problem. The exposure  $I(k)$  measured in units of photon numbers is

$$\begin{aligned} I(k) &= I_R + I_O + I_O + 2\sqrt{I_R I_O} \cos \Phi + N_S \\ &= 9 \times 10^7 \text{ photons} \\ &\text{(with } |N_S| \approx \sqrt{I_R} \text{ because } I_O \ll I_R). \end{aligned}$$

where

$$\begin{aligned} I_R &= \text{intensity of the reference,} \\ I_O &= \text{intensity of the object,} \end{aligned}$$

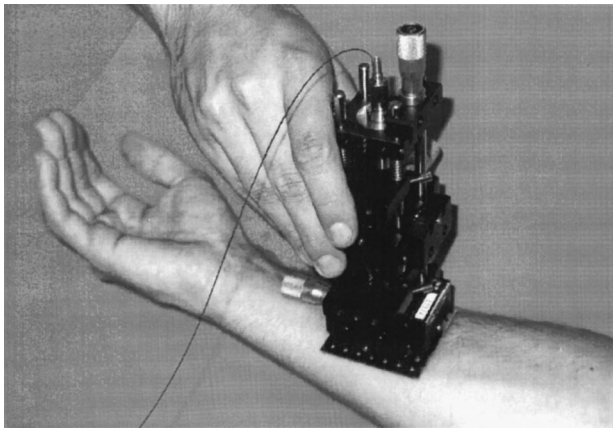


**Fig. 10** Fiber optical implementation of the spectral radar for *in vivo* measurements.

$\Phi = \Phi(k, z)$ : phase between object and reference wave, and

$N_s$  = shot noise.

In order to obtain information about the dynamic range of the spectral radar, we determine the ratio of the maximum and the minimum measurable power  $P$  of the signal from the object. In order to achieve the maximum contrast, the object intensity  $I_{O\_MAX}$  has to be equal to the intensity  $I_R$  and the camera has to be saturated. Now we keep  $I_R$  constant, while  $I_O$  is continuously reduced.  $I_{O\_MIN}$  is the smallest object intensity we still can detect. With  $D = 10 \log(P_{MAX} / P_{MIN}) = 10 \log(I_{O\_MAX} / I_{O\_MIN})$ , the spectral radar has a numerically evaluated dynamic range of  $D = 85$  dB. (The simulation is adapted to the parameters of the experiment.) In practice,  $I_O$  is about  $10^2$  times smaller than  $I_R$ . So we can gain dynamics of 3 dB by using  $I_R$  close to the saturation.

We performed an experiment analogous to the simulation. Again we started with  $I_{O\_MAX} = I_R$ , and the camera was saturated. The object was a mirror.  $I_O$  was successively reduced by putting neutral density filters in the object arm until the signal could just be detected. We measured a dynamic range of  $D = 79$  dB.

### 3.6 IN VIVO MEASUREMENTS

By using the fiber optical setup of Figure 8 we demonstrated several *in vivo* measurements. Figure 10 shows the head of the spectral radar, including the collimation optics, the devices to adjust the reference plane and the depth of focus, and the lateral scanner. Figure 11(a) shows an optogram of the *in vivo* measurement of the hand (inside). The scattering amplitude  $a(z)$ , which is measured at a single line, is shown in Figure 11(b). Along this line we see first a high peak by direct reflection at the surface (depth position  $110 \mu\text{m}$ ). Adjacent to this peak

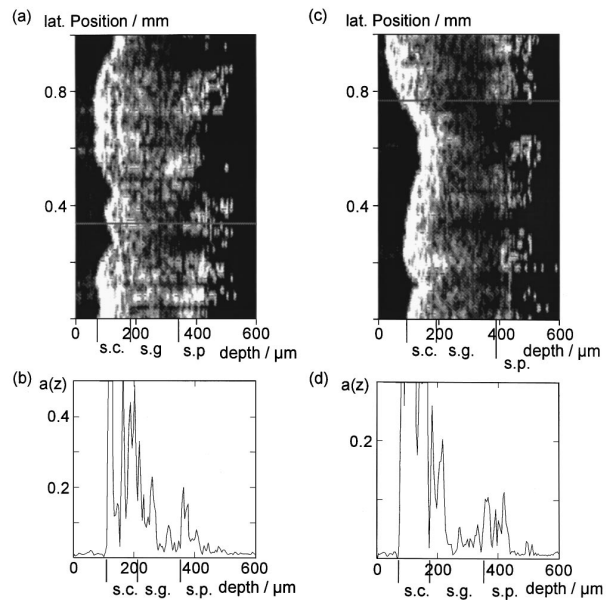


**Fig. 11** Optograms of the hand. (a) Thickness of the layers, evaluated from the true data of the scattering amplitude versus depth; (b) Stratum corneum (s.c.),  $105 \mu\text{m}$ ; stratum germinativum (s.g.),  $140 \mu\text{m}$ , the stratum papillare (s.p.) begins at a depth of  $245 \mu\text{m}$ . Measuring range,  $500 \mu\text{m}$ .<sup>18</sup> (b)  $a(z)$  (Arbitrary units) of normal skin of the hand versus depth for a single measurement. (c) Optogram of the hand with increased moisture content. (d)  $a(z)$  (Arbitrary units) of skin with increased moisture content versus depth for a single measurement. The average extension of the epidermis is about 10%.

we can recognize the stratum corneum (s.c.) by strong scattering (thickness of the s.c.:  $105 \mu\text{m}$ ). The next layer of the skin is the weakly scattering stratum germinativum (s.g.). The thickness of the stratum germinativum in the tomographical cross section is about  $140 \mu\text{m}$ . So the measured thickness of the epidermis (s.c. and s.g.) is  $245 \mu\text{m}$  at the hand. Then the epidermis is followed by the strongly scattering stratum papillare (s.p.), which can be measured up to a depth of about  $500 \mu\text{m}$ .

Such quantitative results can only be derived from the true data of the scattering amplitude versus depth. However, according to the large dynamic range of the measured data, it is not possible to see a high scattering signal from the s.c. as well as the small signal from the inner regions of the s.p. (e.g., at a depth of  $500 \mu\text{m}$ ) in the same diagram. So the question is how to display the data in a single “optogram” (as we call the images to distinguish them from sonograms). This can be only achieved by manipulating the data. The basic idea is to enhance the signal from the large depth by dividing  $a(z)$  by  $e_i = e^{-\alpha_i(z-z_i)}$ . The function  $e_i$  represents the exponential decay of light due to scattering in the layer  $i$ . However, the location of  $z_i$  of the layer boundaries are not the same for different lateral positions. A false  $z_i$  would generate artifacts in the image. So we divide  $a(z)$  by only one exponential function  $e_1$  with one  $e_1 = e^{-\bar{\alpha}(z-z_0)}$ .  $\bar{\alpha}$  is the average

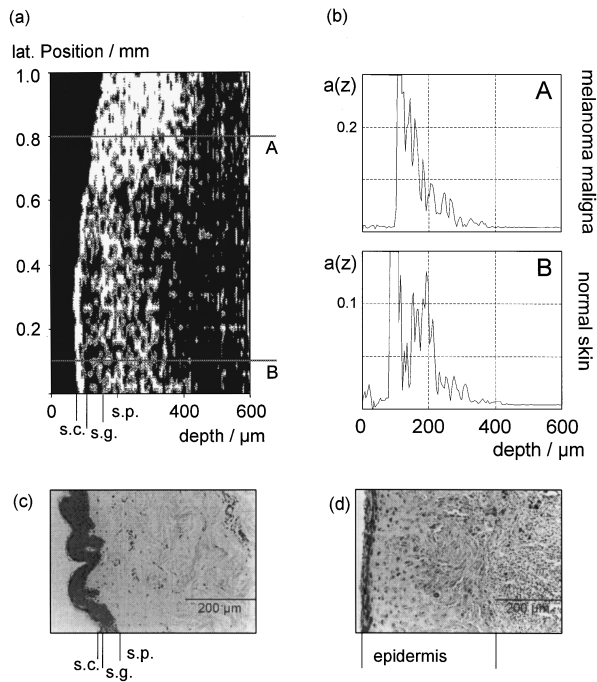


**Fig. 12** Optogram from the lateral boundary region between normal skin and a superficial spreading melanoma (*in vitro*). The melanoma is located on the thigh.<sup>18</sup> (a) Normal skin (bottom) is characterized in the optogram by the different skin layers, and the melanoma (top) is characterized by an extended epidermis with enhanced backscattering. The melanoma is very compact. In the lateral position between  $620\ \mu\text{m}$  and  $900\ \mu\text{m}$ , we can measure the increasing depth of the melanoma in the optogram. (b) The scattering amplitude  $a(z)$  along the line A of the optogram shows homogeneous scattering in the extended epidermis due to the accumulation of melanin. The epidermis has a thickness of  $400\ \mu\text{m}$  (data from the histological image of (d)). In that depth we could not measure the deep boundary of the melanoma. The scattering amplitude  $a(z)$  along the line B of the optogram delivers the thickness of the layers in normal skin: s.c.,  $40\ \mu\text{m}$ ; s.g.,  $50\ \mu\text{m}$ ; depth of the beginning of the s.p.,  $90\ \mu\text{m}$ . (e) Histological image from normal skin. (d) Histological image from the melanoma. The epidermis has a thickness of  $400\ \mu\text{m}$ .

decay constant. In order to get  $\bar{\alpha}$ , we take the sum  $A(z) = \sum_i a_{x_i}(z)$  of the scattering amplitudes  $a_{x_i}(z)$  from all lateral positions  $x_i$ . In  $A(z)$  we fit one exponential function  $e_1$  to the measured data from the skin. A typical value of  $\bar{\alpha}$  from human skin is  $\bar{\alpha} = 13.7\ \text{mm}^{-1}$ . The manipulation has the only purpose of a better presentation. Quantitative results have to be derived from the true data of the scattering amplitude versus depth. It should be pointed out that in spite of the manipulations, all optograms display the correct position and thickness of the skin layers.<sup>18</sup>

We wanted to investigate the influence of increased moisture content on the morphological structure of the skin by OCT. So we performed measurements at a specific location of the hand in the unprepared state and after moisturizing. In order to increase the moisture content, the hand was held in water for 30 min. Figure 11(c) shows the

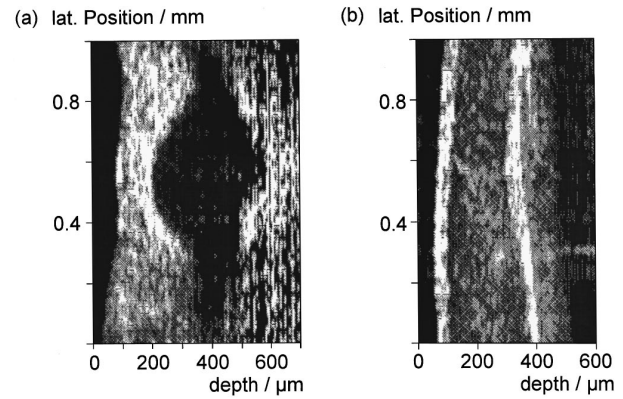


**Fig. 13** Optograms of coronary vessels of a pig heart *in vitro*. (a) Optogram of a vessel filled with isotonic NaCl solution (cross sections perpendicular to the vessel). Thickness of the vessel,  $380\ \mu\text{m}$ . The vessel ruptured on both sides. (b) Optogram of a coronary vessel filled with blood (measurement along the vessel). It can be seen that the thickness decreases from  $290\ \mu\text{m}$  to  $190\ \mu\text{m}$  from the bottom to the top of the optogram. In contrast to Figure 13(a) we see a signal from the light scattered at the blood inside the vessel.

optogram of the skin after the treatment. The epidermis of normal skin has a thickness of about  $245\ \mu\text{m}$  [Figure 11(a)]. After moisturizing, it has increased to  $285\ \mu\text{m}$  [Figure 11(d)]. The average extension of the epidermis is about 10%.

Skin cancer causes increased backscattering through the accumulation of melanin in the cells.<sup>25</sup> This can be measured by the spectral radar.<sup>5</sup> Figure 12(a) displays the optogram of the lateral boundary region of a superficial spreading melanoma (*in vitro*) located on the thigh. The scattering amplitude  $a(z)$  measured at a single line at the melanoma (line A) and the normal skin (line B) is shown in Figure 12(b). It can be seen again that normal skin (bottom) is characterized by different skin layers, and the melanoma (top) is characterized by an extended epidermis with enhanced backscattering. The melanoma is very compact. In the lateral position between  $620$  and  $900\ \mu\text{m}$  we can measure the increasing depth of the melanoma in the optogram. With the light source used we cannot at present measure the thickness of the melanoma in a depth of  $400\ \mu\text{m}$ . The results were confirmed by histological images of normal skin [Figure 12(c)] and the melanoma [Figure 12(d)]. Before surgical removal, we performed *in vivo* measurements of the melanoma and the adjacent normal skin. The *in vivo* measurements display layers in normal skin and enhanced backscattering of the extended epidermis in the pathological skin.<sup>18</sup>

Finally, we measured the thickness of the coronary vessel of a pig heart *in vitro*. Figure 13(a) shows the optogram of a cross section perpendicular to the vessel. The vessel was filled with isotonic NaCl solution (thickness of the vessel:  $380\ \mu\text{m}$ ). However the vessel ruptured on both sides. The measurement of a vessel filled with blood is shown in Figure 13(b) (measurement along the vessel). In

contrast to Figure 13(a), we see a signal from the light scattered at the blood inside the vessel. It can be seen that the thickness decreases from 290 to 190  $\mu\text{m}$  from the bottom to the top of the optogram.

### 3.7 SUMMARY

Spectral radar is an optical sensor for the acquisition of skin morphology. The scattering amplitude  $a(z)$  along one vertical axis from the surface into the bulk can be measured within one exposure. No reference arm scanning is necessary. The experimental determination of the dynamic range is  $D = 79$  dB. We show optograms of *in vivo* measurements of human skin by a fiber optical implementation of the sensor. The thickness of the skin layers at different locations of the body *in vivo* is accurately displayed. For cosmetic application, the influence of increased moisture content can be shown. With the spectral radar, we can distinguish a superficial spreading melanoma from normal skin by the measured optogram. We also measured the thickness of the coronary vessel of a pig heart *in vitro*.

### Acknowledgment

We acknowledge the suggestions and support of Dr. Hoppe, Beiersdorf AG, and Prof. Schaefer and Dr. Dauga from L'OREAL Recherche. We further acknowledge the *in vivo* measurements on patients, interpretation of the results, and valuable suggestions and support supplied by Dr. Kiesewetter, Dermatologische Universitätsklinik und Poliklinik, Erlangen. This work was funded by the BMBF, grant 13N7148.

### REFERENCES

1. M. Fiedler, W.-D. Meier, and U. Hoppe, "Texture analysis of the surface of the human skin," *Skin Pharmacol.* **8**, 252–265 (1995).
2. Th. Dresel, G. Häusler, and H. Venzke, "Three-dimensional sensing of rough surfaces by coherence radar," *Appl. Opt.* **31**, 919–925 (1992).
3. G. Ammon, P. Andretzky, S. Blossy, G. Bohn, P. Ettl, H. P. Habermeier, B. Harand, G. Häusler, I. Laszlo, and B. Schmidt, "New modifications of the coherence radar," *Proc. 3rd Int. Workshop on Automatic Processing of Fringe Patterns* (1997).
4. L. Deck and P. de Groot, "High speed non-contact profiler based on scanning white light interferometer," *Appl. Opt.* **33**, 7334–7338 (1994).
5. M. Bail, A. Eigensee, G. Häusler, J. M. Herrmann, and M. W. Lindner, "3D imaging of human skin—optical *in vivo* tomography and topology by short coherence interferometry," *Proc. SPIE* **2981**, 64–75 (1997).
6. G. Ammon, P. Andretzky, G. Bohn, G. Häusler, J. M. Herrmann, and M. W. Lindner, "Optical coherence profilometry

- (OCP) of human skin *in vivo*," *Proc. SPIE* **3196** (1997).
7. X. Clivaz, F. Marquis-Weible, R. P. Salathe, R. P. Nowak, and H. H. Gilgen, "High-resolution reflectometry in biological tissues," *Opt. Lett.* **17**(1), 4–6 (1992).
8. J. A. Izatt, M. R. Hee, G. M. Owen, E. A. Swanson, and J. G. Fujimoto, "Optical coherence microscopy in scattering media," *Opt. Lett.* **19**(8), 590–592 (1994).
9. A. F. Fercher, "Optical coherence tomography," *J. Biomed. Opt.* **1**(2), 157–173 (1996).
10. A. Baumgartner, B. Möller, Ch. K. Hitzberger, W. Drexler, and A. F. Fercher, "Measurements of the posterior structures of the human eye *in vivo* by partial coherence interferometry using diffractive optics," *Proc. SPIE* **2981**, 85–93 (1997).
11. E. Lankenau, J. Welzel, R. Birngruber, and R. Engelhardt, "In vivo tissue measurements with optical low coherence tomography," *Proc. SPIE* **2981**, 78–84 (1997).
12. R. Lazar, H. Brunner, and R. Steiner, "Optical coherence tomography (OCT) of human skin with a slow-scan CCD-camera," *Proc. SPIE* **2925**, 143–151 (1996).
13. A. Eigensee, G. Häusler, J. M. Herrmann, and M. W. Lindner, "A new method of short-coherence-interferometry in human skin (*in vivo*) and in solid volume scatterers," *Proc. SPIE* **2925**, 169–178 (1996).
14. J. M. Schmitt, A. Knüttel, M. Yadlowsky, and M. A. Eckhaus, "Optical coherence tomography of a dense tissue: statistics of attenuation and backscattering," *Phys. Med. Biol.* **39**, 1705–1720 (1994).
15. A. F. Fercher, C. K. Hitzberger, G. Kamp, and S. Y. El-Zaiat, "Measurement of intraocular distances by backscattering spectral interferometry," *Opt. Comm.* **117**, 43–48 (1995).
16. G. Häusler, German patent DE 41 08 944 (1991).
17. M. Bail, G. Häusler, J. M. Herrmann, M. W. Lindner, and R. Ringler, "Optical coherence tomography with the spectral radar—fast optical analysis in volume scatterers by short coherence interferometry," *Proc. SPIE* **2925**, 298–303 (1996).
18. M. Bail, G. Häusler, J. M. Herrmann, F. Kiesewetter, M. W. Lindner, and A. Schutz, "Optical coherence tomography by spectral radar for the analysis of human skin," *Proc. SPIE* **3196** (1997).
19. U. Haberland, P. Jansen, V. Blazek, and H. J. Schmitt, "Optical coherence tomography of scattering media using frequency modulated continuous wave techniques with tunable near-infrared laser," *Proc. SPIE* **2981**, 20–28 (1997).
20. S. R. Chinn, E. A. Swanson, and J. G. Fujimoto, "Optical coherence tomography using a frequency-tunable optical source," *Opt. Lett.* **22**(5), 340–342 (1997).
21. G. Häusler, J. M. Herrmann, R. Kummer, and M. W. Lindner, "Observation of light propagation in volume scatterers with  $10^{11}$ -fold slow motion," *Opt. Lett.* **21**(14), 1087–1089 (1996).
22. V. V. Tuchin, "Coherent and polarimetric optical technologies for the analysis of tissue structure," *Proc. SPIE* **2981**, 120–159 (1997).
23. J. Müller, *Poggendorfs Annalen* **69**, 98 (1846).
24. E. Wolf, "Three-dimensional structure determination of semi-transparent objects from holographic data," *Opt. Comm.* **1**, 153–156 (1969).
25. A. Sergeev, N. Gladkova, F. Feldchtein, V. Gelikonov, G. Gelikonov, L. Snopova, J. Ioannovich, K. Frangia, T. Pirza, I. Antoniou, A. Dunn, and R. Richards-Kortum, "Melanin effect on light scattering in tissues: from electrodynamics of living cell to OCT imaging," *Proc. SPIE* **2981**, 58–63 (1997).